High dose of baicalin or baicalein can reduce tight junction integrity by partly targeting the first PDZ domain of zonula occludens-1 (ZO-1)

Misaki Hisada[1#], Minami Hiranuma[1], Mio Nakashima[2], Natsuko Goda[1], Takeshi Tenno[1,3], and Hidekazu Hiroaki[1,2,3,*]

From the [1]Graduate School of Pharmaceutical Sciences, Nagoya University, Furocho, Chikusa, Nagoya, Aichi, 464-8601, Japan, [2]Department of Biological Sciences, Faculty of Science, Nagoya University, [3]BeCerllBar, LLC., Nagoya, Aichi, Japan.

Running title: *Baicalin reduces tight junction by targeting the first ZO-1 PDZ domain*

#Present address: Research Center, Koken Co.,Ltd., 2-13-10, Ukima, Kita-ku, Tokyo, 115-0051, Japan

*To whom correspondence should be addressed: Hidekazu Hiroaki: Graduate School of Pharmaceutical Sciences, Nagoya University, Furocho, Chikusa, Nagoya, Aichi, 464-8601, Japan; hiroaki.hidekazu@f.mbox.nagoya-u.ac.jp; Tel. +81(52)789-4535; Fax. +81(52)-747-6816

ABSTRACT

The tight junction (TJ) is the apical-most intercellular junction complex, serving as a biological barrier of intercellular spaces between epithelial cells. The TJ's integrity is maintained by a key protein–protein interaction between C-terminal motifs of claudins (CLDs) and the postsynaptic density 95 (PSD-95)/discs large/zonula occludens 1 (ZO-1; PDZ) domains of ZO-1. Weak but direct interaction of baicalin and its aglycon, baicalein—which are pharmacologically active components of Chinese skullcap (*Radix scutellariae*)—with ZO-1(PDZ1) have been observed in NMR experiments. Next, we observed TJ-mitigating activity of these flavonoids against Madin-Darby canine kidney (MDCK) II cells with the downregulation of subcellular localization of CLD-2 at TJs. Meanwhile, baicalein—but not baicalin—induced a slender morphological change of MDCK cells' shape from their normal cobblestone-like shapes. Since baicalin and baicalein did not induce a localization change of occludin (OCLN), a "partial" epithelial–mesenchymal transition (EMT) induced by these flavonoids was considered. SB431542, an ALK-5 inhibitor, reversed the CLD-2 downregulation of both baicalin and baicalein, while SB431542 did not reverse the slender morphology. In contrast, the MEK/ERK inhibitor U0126 reversed the slender shape change. Thus, in addition to inhibition of the ZO-1–CLD interaction, activation of both transforming growth factor-β (TGF-β) and MEK/ERK signaling pathways have been suggested to be involved in TJ reduction by these flavonoids. Finally, we demonstrated that baicalin enhanced the permeability of fluorescence-labeled insulin via the paracellular pathway of the Caco-2 cell layer. We propose that baicalin, baicalein, and *Radix scutellariae* extract are useful as drug absorption enhancers.

Keywords

PDZ domain inhibitor, tight junction, zonula occludens-1, NMR, baicalin, absorption enhancer, TGF-β signaling pathway, epithelial cell barrier

1. Introduction

The tight junction (TJ), or zonula occludens (ZO), is the apical-most intercellular junction complex found in epithelial and endothelial cells (Förster, 2008; Furuse et al., 2002; Tsukita et al., 2001). TJs' relevant physiological function is to limit the free translocation of solvents, solutes, and cells through the paracellular pathway. TJs are complex structures composed of integral membrane proteins, and scaffold proteins that are connecting membranous components to the cortical actin ring. The membranous TJ components include occludin (OCLN) and the members of the claudin (CLD) family, latter of which form paracellular barriers (Fanning et al., 1999; Furuse et al., 1998; Paris et al., 2008). CLDs are connected to the postsynaptic density 95 (PSD-95)/discs large/ZO-1 (PDZ) domain-containing proteins, such as ZO-1, ZO-2, and ZO-3 (Itoh et al., 1999). The molecular functions of these ZO proteins are thought to tether membrane proteins using their multiple PDZ and other domains (González-Mariscal et al., 2003). Although their functions in TJ maintenance and biogenesis are seemingly redundant, ZO-1 seems more important than the others (Adachi et al., 2006; Ikenouchi et al., 2007; Umeda et al., 2006). In contrast, C-terminal residues of CLDs correspond critical physiological role. The mutations in C-terminal PDZ-binding motifs (PBMs) of CLDs have shown to result in defective phenotypes (Furuse, 2009). It has been shown that the first PDZ domain of ZO-1 (ZO-1(PDZ1)) is responsible for CLD recognition (Itoh et al., 1999). This suggests the interactions between the ZO-1(PDZ1) and CLD are a potential target for mitigating the TJ-based biological barriers.

The PDZ domain is a compact, globular module of 90–100 amino acid residues, dedicated to protein–protein interaction. The canonical PDZ domains specifically bind to the C-terminal PBMs of other proteins (Fanning and Anderson, 1996; Harris and Lim, 2001; Jiang et al., 2013; Sheng, 2001). Notably, approximately 20% of PDZ domains can also bind the head group of phosphatidyl inositol phosphates (PIPs)(Zimmermann, 2006). We previously found that ZO-1(PDZ1) shares its canonical CLD binding cleft to PIPs interaction, and the PDZ–CLD and PDZ–PIP interactions were mutually exclusive. We showed that PI3 kinase inhibitor LY-294002 enhanced the accumulation of CLD-7 to TJs at the

apicolateral membrane area of Madin-Darby canine kidney (MDCK) II cells, probably by decreasing concentration of PIPs at the apical membrane site (Hiroaki et al., 2018).

In this study, we aimed to discover a naturally occurring inhibitor against ZO-1(PDZ1)-CLDs interaction as a candidate for tight junction modulators. We were encouraged by Tang's report (Tang et al., 2004), which demonstrated flavonoids from *Radix scutellariae* could bind the PDZ2 domain of human PSD-95 protein and be developed as therapeutic agents against stroke. We are aware of the similarity between the ZO-1(PDZ1) and PSD-95(PDZ2) domains at both the sequence and three-dimensional structure levels (Fig. 1). We found that baicalin and baicalein showed specific binding to ZO-1(PDZ1) by using NMR methods. These flavonoids showed TJ mitigating activity. Possible molecular mechanisms of the flavonoids are also investigated.

2. Materials and methods

2.1. Materials

Chrysin, wogonin, hesperetin, rutin, daidzein, and U0126 were purchased from Wako Pure Chemical Industries (Osaka, Japan). Baicalin, baicalein, naringenin, and D-glucuronic acid were acquired from Tokyo Kasei Kogyo (Tokyo, Japan), while (−)-epicatechin and cyanidin chloride were from Nagara Science Co. Ltd. (Gifu, Japan). Delphinidin chloride was obtained from Nacalai Tesque (Kyoto, Japan). Daidzin was acquired from Adooq BioScience (Irvine, CA, USA), while astilbin was purchased from Abcam (Cambridge, MA, USA); SB431542 was purchased from Cayman Chemical Company (Ann Arbor, MI, USA).

The rabbit anti-CLD-2 and rabbit anti-OCLN antibodies obtained were from Sigma-Aldrich (St. Louise, MO, USA). Rabbit anti-ZO-1 antibodies were from Invitrogen (Carlsbad, CA, USA). Mouse anti-β-actin antibody was purchased from Abcam. Rhodamine-phalloidin was from Cytoskeleton, Inc (Denver, CO, USA). For immunofluorescent microscopy, anti-rabbit immunoglobulin G (IgG) and F(ab')2 fragment-Cy3 antibody were obtained from Sigma-Aldrich. For Western blotting analysis, anti-rabbit and mouse IgG horseradish peroxidase (HRP) conjugates were acquired from Promega (Madison, WI, USA).

All other reagents were of the highest grade of purity available.

2.2. Protein expression and purification

Expression and purification of mouse ZO-1(PDZ1) (residues 18–110) was previously described (Hiroaki et al., 2018; Umetsu et al., 2011). In brief, the recombinant glutathione-S-transferase (GST)-tagged form of ^{15}N-labeled mouse ZO-1(PDZ1) was expressed by *Escherichia coli* BL21 (DE3) in 2 l M9 minimal media with [^{15}N]-ammonium chloride as the sole nitrogen and sources, supplemented with divalent cations and vitamins at 20 °C. The fusion protein was captured by affinity purification on glutathione-Sepharose FF (GE Healthcare Life Sciences Corp, Piscataway, NJ, USA). Production of ^{15}N-labeled ZO-1(PDZ1) was achieved by on-column digestion by PreScission™ Protease followed by gel filtration chromatography using a Superdex 75 column (GE Healthcare Life Sciences Corp.).

2.3. NMR titration experiments

For examining the direct binding of the flavonoids to ZO-1(PDZ1), a series of 2D ^{1}H-^{15}N heteronuclear single quantum coherence spectroscopy (HSQC) spectra with WATERGATE water suppression (Piotto et al., 1992) was recorded at 25°C, in 5% D_2O–95% H_2O containing 20 mM MES buffer (pH 5.9). In the titration, 0, 2, and 10 molar equivalences of baicalin, baicalein, and wogonin were added to 0.1 mM ^{15}N-labeled ZO-1(PDZ1). All the normalized chemical shift changes in the ^{1}H-^{15}N HSQC spectra upon ligand titration were calculated as $\Delta\delta_{normalized} = \{\Delta\delta(^{1}H)^2 + [\Delta\delta(^{15}N)/6]^2\}^{1/2}$, where $\Delta\delta(^{1}H)$ and $\Delta\delta(^{15}N)$ are chemical shift changes in amide proton and amide nitrogen, respectively. Visualization of the normalized chemical shift changes upon the compound binding was performed by the program PyMOL (Schrödinger, LLC, 2015) onto the ribbon representation of PDB code 2RRM. Each threshold value was calculated using the method developed by Schumann et al. (2007).

2.4. Preparation of Chinese skullcap extract

Dried, chopped root of *Scutellariae baicalensis* Georgi (Japanese Pharmacopoeia certificated grade)

was purchased from Tochimoto Tenkaido Co., Ltd. (Osaka, Japan). Ten grams of the plants root were extracted with 50 ml of warm H_2O at 80°C for 1 h twice in a stirred flask. Extracts were put together and used as water extract. To the same amount of the water extract, 1 M HCl was added to adjust the pH to 2.0. The solution was kept at 80°C for 30 min, and the precipitants were collected by a filter paper with vacuum filtration. The precipitants were washed with 95% ethanol three times and dried (Extract A). On the other hand, 10 g of the plants root was extracted with 100 ml of warm 80% ethanol at 60°C for 12 h three times in a stirred flask. The extracts were put together and evaporated. Approximately 0.3 g of crude flavonoids (from a total of 0.5 g) was redissolved in 100 ml of H_2O and extracted twice using 100 ml of ethanol acetate; the organic phase was then collected and evaporated (Extract B).

2.5. HPLC analysis of Chinese skullcap extracts

Each 1 mg of extract was analyzed by a reversed-phase (RP) HPLC (GL-5452A PDA detector equipped with a GL-7410 pump, GL Sciences Inc., Tokyo, Japan) at 350 nm using an Inertsil® ODS-4 column (GL Sciences Inc.) with a linear gradient of H_2O containing 0.5% trifluoro-acetic acid (TFA) and 80% acetonitrile in 0.5 % TFA. The retention times of three of the four major flavonoids—baicalin, baicalein, and wogonin—were defined using commercially purchased standard samples. Peak 2 was purified by RP-HPLC and analyzed by mass spectrometry (FAB-MS, JMS-700, JEOL Co. Ltd., Tokyo, Japan), with a result of 459 (m/z); it was identified as wogonoside.

2.6. Cell culture

MDCK II cells were cultured in Dulbecco's modified Eagle's medium (DMEM) supplemented with 10% fetal bovine serum (FBS; Biosera, Ringmer, UK) and 1 % penicillin/streptomycin (Difco Laboratories, MI, USA) at 37°C with 5% CO_2. Aliquots of 3.0×10^4 cells were plated on each well of a 6-well x 35-mm plate (Corning Japan, Tokyo, Japan), and the culture medium was changed every 2 days. Three days after plating, the culture medium was changed to the same medium containing 50 and 100 μM of baicalin and baicalein or the indicated amount of Chinese skullcap extract. After 48 h of exposure to the

compounds or extracts, the cells were subjected to immunofluorescence, cell morphology, Western blotting, or real-time PCR analysis. Cells exposed to 0.1% dimethyl sulfoxide (DMSO) were always used as a control. Caco-2 cells were cultured in Minimum Essential Medium Eagle (Sigma-Aldrich) supplemented with 10% FBS (Biosera) and 1% penicillin/streptomycin (Gibco, UK), and 1% MEM-NEAA (Gibco) at 37°C with 5% CO_2.

2.7. Immunofluorescence microscopy

The cells were fixed with cold 1 x phosphate-buffered saline containing 4% paraformaldehyde and incubated with primary antibodies for 24 h at 4°C. Primary antibody dilutions were as follows: CLD2 and ZO-1, 1:200; OCLN, 1:1000. Rhodamine-phalloidin dilution for actin staining was 1:1000. The cells were then incubated with secondary antibodies for 1 h at room temperature. Cy3-conjugated secondary antibody was used at a dilution of 1:10,000. The fluorescence images were obtained using fluorescence microscopy equipped with a color CCD camera (IX-71 and DP-70, respectively; Olympus, Tokyo, Japan; scale bar: 20 μm).

2.8. Cell morphology analysis

For characterizing the morphological parameters of the cell shapes, differential interference contrast (DIC) images were digitalized and analyzed by ImageJ software (National Institutes of Health). The cell edge was traced manually, and the cell area was quantified by the "analyze measure" command in the "polygon selection" menu. The longer and shorter axes were quantified in the "straight line selections" menu. From each viewing area, five cells were randomly chosen and analyzed. All the parameters were normalized against the corresponding values from the control cells.

2.9. Western blotting

Aliquots of 3.0 x 10^4 MDCK II cells were plated on each well of a 6-well x 35-mm plate (Corning Japan), and the culture medium (DMEM) containing 100 μM of the compounds of interest and a final

concentration of 0.1% of d6-DMSO were added. The cells were harvested after 48 h of incubation under 5% CO_2 at 37°C. The cells were rinsed twice with DMEM medium without serum and recovered with 100 μL of the buffer containing sodium dodecyl sulfate (SDS). The cells were disrupted by a mild sonication using Bioruptor (Cosmo Bio, Tokyo, Japan) for 3 min (duty cycle 50%). All the crude protein samples were analyzed by SDS–polyacrylamide gel electrophoresis (SDS-PAGE). The gel was washed with the buffer containing 25 mM Tris-HCl (pH 7), 192 mM glycine, and 20% methanol and electroblotted to PVDF membrane (ATTO, Tokyo, Japan). The PVDF membrane was blocked by 3% skim milk and incubated with the primary antibodies overnight. Primary antibody dilutions were as follows: CLD2 1:200; β-actin, 1:5000. The membrane was then washed twice and treated with the corresponding secondary antibody with 1:10000 dilution. The proteins were illuminated by Chemi-Lumi One Super solution (Nacalai Tesque) and detected using the LAS3000 mini imaging analyzer system (Fuji Film, Tokyo, Japan).

2.10. Real-time PCR

Aliquots of 1.5 x 10^4 MDCK II cells were plated on each well of a 96-well plate (Corning Japan) and incubated for 24 h. Then DMEM culture media containing 100 μM flavonoids with a final concentration 0.1 % of d_6-DMSO were added. The cells were harvested after 48 h of incubation under 5% CO_2 at 37°C. The cells were rinsed with medium and subjected to cDNA preparation using SuperPrep® Cell Lysis & RT Kit for qPCR (Toyobo, Co., Tokyo, Japan) based on the manufacturer's instructions.

Quantitative real-time PCR was performed using the PCRMax Eco™ Real Time PCR System (AS ONE Corporation, Osaka, Japan). The CLD-2 gene was analyzed with the specific primers (Fw 5′-CGCTCCGACTACTATGACTCCT-3′ and Rev 5′-GGCCTTGGAG AGCCTCTAGT-3′). An aliquot of 1 μl of template cDNA with 1 μl of forward and reverse primers was mixed with 5 μL of THUNDERBIRD® SYBR® qPCR Mix (Toyobo) and adjusted to a total solution volume to 10 μl.

2.11. Paracellular permeation assay

Caco-2 cells were cultured to a tight monolayer on the upper transwell filter of a Millicell-24 cell culture plate (Merck-Millipore, Darmstadt, Germany) and maintained for approximately 14 days until stable transepithelial electrical resistance (TEER) was achieved. The standard culture medium (Minimum Essential Medium Eagle, Sigma, supplemented with 10% FBS (Biosera, Kansas City, MO, USA), 1% penicillin/streptomycin (Gibco), and 1% MEM-NEAA (Gibco) was used and changed every 2 days. The TEER of the cell monolayer was measured with an epithelial volt-ohmmeter (Millicell® ERS-2, Merck-Millipore, USA). For assessing the paracellular permeability, cells with stable TEER on the filter were incubated with above standard medium (400 μl) supplemented with 300 μM of baicalin or baicalein or 0.3% DMSO and 2.5 μg/ml fluorescein isothiocyanate (FITC)-insulin (Sigma) as the paracellular flux tracer. Subsequently, 800 μl of the standard culture medium was added to the basal side chamber. At given times, each 100 μl of sample from the basal side was taken and placed in a black 96-well plate (Perkin-Elmer, Norwalk, CT, USA). The fluorescence was measured with an EnSpire plate reader (Perkin-Elmer) excited at 488 nm and emitted at 509 nm.

3. Results

3.1. Computational inspection of potential interaction between flavonoids and ZO-1(PDZ1)

In this study, we initially hypothesized that either baicalin itself or one of any other related flavonoids can bind ZO-1(PDZ1). In the original Tang's report, two of four baicalin-related flavonoids including flavone 7-glucuronides isolated from extract of Chinese skullcap (*R. scutellariae*), baicalin and nor-wogonoside, bound to PSD-95(PDZ2), as examined by the NMR titration experiments. The chemical shift perturbations (CSPs) induced by these flavonoids supported that the molecules bound the canonical ligand binding cleft of PSD-95(PDZ2). In order to assess the possibility of flavonoids and ZO-1(PDZ1), we compared the shape and the electrostatic charge distribution of the PDZ domains, PSD-95(PDZ2) and ZO-1(PDZ1) (Fig. 1). Both properties around the canonical ligand binding cleft resemble each other. In detail, except that the charge distributions of the top of the left rim outside the binding pocket are opposite each other (negatively charged in ZO-1(PDZ1) and positively charged in PSD-95(PDZ2), respectively), the length,

width, depth, and overall shape of the two binding pockets are similar (indicated by hexagons in Fig. 1B and 1C). In addition, the right-side bottom corners of the pockets of both the PDZ domains were positively charged to form the carboxylate binding site (indicated by arrows in Fig. 1B and 1C). Thus, we concluded some flavonoids are possible to bind ZO-1(PDZ1).

In addition, contribution of the carboxylic group of glucuronic acid in baicalin to PDZ domains drew our attention because PDZ domains widely possess affinity against the C-terminal carboxylate group of their physiological ligand peptides. In contrast, a wide variety of combinations of hydroxy groups on the A, B, and C rings of the flavonoid moiety may serve as a determinant for specificity. We chose 14 molecules, including flavonoids, iso-flavonoids, and glucuronic acid alone, as the candidate molecules (Supplementary Fig. 1). All these molecules were examined by NMR titration experiments with 0.1 mM ^{15}N-labeled mouse ZO-1(PDZ1) in the presence of 0.2 mM flavonoids. Some of the flavonoids were further examined by increasing the ratio (data not shown).

3.2. Direct interaction of baicalin and baicalein to ZO-1(PDZ1)

Specifically, 9 molecules (baicalin, baicalein, hesperetin, naringenin, cyanidin, delphinidin, daidzein and glucuronic acid) among the 14 examined molecules showed some level of CSPs on the canonical ligand binding site of ZO-1(PDZ1). Superimposed ^{1}H-^{15}N two-dimensional spectra shows a weak but direct interaction between ZO-1(PDZ1) and baicalin or baicalein, respectively (Fig. 2A and 2B). For others, the data are not shown and will be published elsewhere. The chemical structures of baicalin and baicalein are summarized in Fig. 2C. ZO-1(PDZ1) adopts a canonical PDZ domain fold, comprising 6 β strands and 1 α helix (Appleton et al., 2006). CLD C-terminal PBMs bind to the canonical ligand binding cleft between α1 and β2 (Nomme et al., 2015). The normalized chemical shift changes were calculated, plotted (Fig. 2D and 2E) and mapped onto the solution structure of ZO-1(PDZ1) (PDB: 2RRM; Fig. 2F and 2G). The data showed that both baicalin and baicalein bound to the canonical ligand binding cleft of ZO-1(PDZ1). The CSP induced by baicalin is larger than that of baicalein. Thus, the affinity between baicalin and ZO-1(PDZ1) is assumed to be stronger than that of baicalein.

We continued these NMR titration experiments with increased amounts of baicalin and baicalein and tried to estimate the K_d values of each compound from the saturation curve. We succeeded in estimating the K_d of baicalin as 1.8 mM (data not shown). We failed to estimate the K_d of baicalein due to its weaker interaction. The result suggested that the glucuronic acid moiety is disposable for baicalin–PDZ interaction but contributes to binding. Indeed, we titrated ZO-1(PDZ1) with glucuronic acid alone and observed weak but certain CSPs (data not shown). Wogonin, a related flavonoid of Chinese skullcap, was also examined, but it did not induce any CSPs (Fig. 2H). Thus, the numbers and positions of hydroxyl/hydroxy-methyl groups on the A ring of flavonoid seemed to be important for ZO-1(PDZ1) binding (Fig. 2C).

3.3. Reversible TJ modulating activity of baicalin and baicalein

We subsequently examined the TJ reduction by the two flavonoids—baicalin and baicalein. For this purpose, MDCK II cells were chosen for the model system to observe TJs. CLD-2 was selected as the TJ marker because this is one of the most abundant CLDs in MDCK II cells, and it is historically well studied (Furuse et al., 2001). After exposure of the 100 μM flavonoids, CLD-2 localized at the cell–cell junction drastically vanished, and only internalized portion was visible (Fig. 3B and 3D). After removal of the flavonoids with fresh medium, CLD-2 reappeared at the intercellular junction (Fig. 3C and 3E); thus, the TJ reduction activity of baicalin and baicalein was reversible. We did not see any significant damage of MDCK cells on the baicalin treatment by bright field microscopy observation (Fig. 3G). However, we found a morphological change from the cobblestone-like shape to a fibroblast-like slender shape with baicalein treatment (Fig. 3I). This change is also significant in ZO-1 and OCLN stained images (see Fig. 5F and 5I). This change seemed partly irreversible, and we could still observe the slender-shaped cells to some extent after 48 h of washing out (Fig. 3J).

We further examined the mechanisms of TJ inhibition by baicalin and baicalein. Western blot analysis of CLD-2 of baicalin/baicalein-treated MDCK II cells is indicated in Fig. 4A. In this experiment, a significant decrease of the CLD-2 protein was induced by both baicalin and baicalein. However, quantitative analysis of the CLD-2 level by western blotting was difficult because we failed to reproducibly observe the

level of the control cells (see Fig. 4B, lane 1). After 48 h of washing by the medium without flavonoids, the CLD-2 levels were increased. The results are consistent with the previous immunofluorescent microscopic observation. We estimated the expression level of CLD-2 mRNA by real time (RT)-PCR analysis (Fig. 4C). Surprisingly, the CLD-2 level was suppressed by transcriptional control. We did not expect this result because our initial working hypothesis, based on our observation of mutual competitive interaction between ZO-1-CLDs and ZO-1-phosphatidyl inositol phosphates, was that only an inhibition of protein–protein interaction between CLD-2 and ZO-1(PDZ1) would occur due to the action of the flavonoid compounds (Hiroaki et al., 2018). The results led us to consider other unknown signaling pathways stimulated by baicalin and baicalein.

3.4. Baicalein but not baicalin induced a partial fibroblast-like morphology change in MDCK cells

Since baicalein induced the fibroblast-like slender cell shape change of MDCK cells, we examined whether the epithelial–mesenchymal transition (EMT) occurred. Although there is no published report suggesting that baicalein (or baicalin) has EMT-promoting activity, we identified Cai et al.'s (2017) study, in which high-dose baicalin activated the TGF-β signaling pathway in the Sprague–Dawley (SD) rat kidney. These researchers also reported increased collagen synthesis and fibrosis in the kidney via high-dose administration of baicalin. Since kidney fibrosis is one of the well-studied diseases caused by pathological EMT (Liu, 2010), we hypothesized that baicalein (and baicalin to some extent) induced TGF-β expression in MDCK cells, and we consider that the fibroblast-like cell shape change may be a secondary effect of TGF-β. To assess the possibility of EMT event, we examined the other TJ-related proteins, including ZO-1 and OCLN, by immunofluorescent microscopy (Fig. 5). In addition, the actin cytoskeleton was observed. In paraformaldehyde-fixed cells, the morphological change of MDCK cells induced by baicalein was more significant than by baicalin in bright-field observation of the living cells (Fig. 5C, 5F, 5I and 5L compared with 5B, 5E, 5H and 5K, respectively).

The cobblestone-like rounded cell shape was enlarged and distorted when treated by baicalein. In cells treated with both baicalin and baicalein, the subcellular localization of ZO-1 and OCLN were still observed

at the lateral membrane near the intercellular TJ space. This is a strong indication that EMT was not completed at this stage (Fig. 5E, 5F, 5H, and 5I). From these results, we concluded that the baicalein-induced morphological change of MDCK cells is not a case of complete EMT because the disappearance of ZO-1 and OCLN from TJ is one of the critical indications of EMT. When observing the actin cytoskeleton, a clear cortical actin ring was observed in the non-treated MDCK cells (Fig. 5J). In both the cells treated with baicalin and baicalein, only a slight perturbation of the clear cortical actin ring was observed, but this change was not significant. Thus, we assumed that the actin cytoskeleton regulation pathway is not the direct target of baicalin and baicalein.

3.5. Involvement of TGF-β and MEK/ERK pathways in TJ inhibition by baicalin and baicalein

Since Cai et al. (2017) reported that the increased expression of TGF-β and activation of the TGF/Smad signaling pathway was induced by high-dose administration of baicalin, we examined whether this pathway is also involved in baicalin/baicalein-induced CLD downregulation and baicalein-induced morphological change in MDCK cells. For this purpose, we investigated the effect of SB431542, a TGF-β receptor (ALK-5) inhibitor, on baicalin/baicalein-treated MDCK cells. Controversially, the report has suggested that baicalein can inhibit the ERK signaling pathway (Li et al., 2010), although ERK is one of the critical signaling milestones during TGF-β-induced EMT (Xie et al., 2004). Accordingly, we examined whether SB431542 and U0126, MEK/ERK inhibitor, could reverse the pharmacological effect of baicalin and baicalein. As shown in Fig. 6, exposure of SB431542 succeeded in reversing the disappearance of CLD-2 from the intercellular contact area induced by both baicalin (Fig. 6A-d) and baicalein (Fig. 6A-f). However, the cell shape change induced by baicalein was not completely reversed (Fig. 6A-f and 6B-f). In contrast, although U0126 failed to reverse the disappearance of CLD-2 (Fig.6A-j and 6A-l), it reversed the morphological change induced by baicalein (Fig. 6A-l and 6B-l).

To clarify the morphological change induced by these flavonoids and inhibitors, the lengths of the long and short axes in the bright-field microscopic observation of the MDCK cells were analyzed (Fig. 7A–D). The baicalein treatment induced 170% and 120% increases of the long and short axes of the cell,

respectively (Fig. 7A, 7B). After the baicalein was washed away, the effects partly remained. The addition of the ERK pathway inhibitor U0126, but not ALK-5 inhibitor SB431542, reversed the baicalein-induced morphological changes, especially the elongation of the long cell axis (Fig. 7C, 7D).

3.6. Different extraction methods of Radix scutellariae alter the morphology of MDCK cells

Chinese skullcap (*R. scutellariae*, also known as *Scutellariae baicalensis*) is a herb with a long history of medicinal use in China (as a traditional Chinese medicine, TCM), as well as Japan (as a Japanese herbal medicine). Interestingly, both "huang qin" in Chinese and "ou-gon" in Japanese have the same meaning—the "golden herb." The dried root of Chinese skullcap is used as the source of extraction, and depending on the extraction method, the extracts may contain both baicalin and baicalein in varied content. We prepared typical Chinese skullcap extracts by distinct protocols and examined their different pharmacological effects on MDCK cells. Fig. 8A–C shows the chart of reversed-phase high-performance liquid chromatography (HPLC) of the Chinese skullcap extracts. When extracting hot water followed by acid precipitation, baicalin became the dominant component (Fig. 8B, "extract A"). When extracting 80% EtOH followed by ethyl acetate extraction, two major glycosides were eliminated, while baicalein and wogonin became major components (Fig. 8C, "extract B"). The cellular activity of these extracts was examined by bright-field microscopy as well as immune-fluorescent microscopy. Both the extracts showed TJ-mitigating activity on MDCK II cells that was similar to the effect induced by the isolated flavonoids, baicalin and baicalein, as expected (Fig. 8H and 8I). In addition, the morphological change toward a slender cell shape was reproduced only by extract B, in which baicalein was dominant (Fig. 8F). Thus, although Chinese skullcap extracts are useful as TJ-mitigating medicine, the extraction method must be regulated to avoid cellular morphological change.

3.7. Drug absorption enhancement activity of baicalin and baicalein for the Caco-2 cell model

Finally, we investigated the drug absorption enhancement activity of the two flavonoids. The development of "injection-needle-free" drug delivery methods for medium-molecular-sized drugs, such as

peptide hormones, cytokines, cyclic peptides, peptide vaccines, and antisense oligonucleotide therapeutics, is an emerging technology. Here, we focus on the potential application of Chinese skullcap extracts as a drug absorption enhancer, since this plant has a history of human administration that is longer than 2000 years and the risks of its medical use have been extensively studied. To demonstrate the activity of drug permeability enhancement of baicalin and baicalein, paracellular permeability of insulin over the Caco-2 cell monolayer as an intestinal mucosal barrier model was examined (Fig. 9). Both compounds showed +20% enhancement of insulin, demonstrating their potential for developing the oral administration of insulin to diabetes patients.

4. Discussion

In this study, we demonstrated the barrier-opening activity of the paracellular pathway of baicalin and baicalein. Both flavonoids showed weak but pocket-specific binding to ZO-1(PDZ1). These interactions were partly expected because baicalin has been reported to bind the other PDZ domain, PSD-95(PDZ2) (Tang et al., 2004), and the molecular surfaces of ZO-1(PDZ1) and PSD-95(PDZ2) are closely related (Fig. 1B and 1C). Since the dominant molecular determinants for the conventional PDZ interaction motif is the carboxylate group of its C-terminus, we initially assumed the carboxylate group of the glucuronate of baicalin was the most important pharmacophore for ZO-1(PDZ1) binding. However, even without glucuronate moiety, baicalein still weakly bound ZO-1(PDZ1). Thus, the planar flavonoid moiety with certain spatial arrangement of two or more hydroxyl groups is sufficient for interaction, while the glucuronate moiety may only assist binding (Fig. 2).

Subsequently, we showed the TJ-mitigation activity of baicalin and baicalin at MDCK II cells. This observation is consistent with the fact that the first PDZ domain of ZO-1 and its interaction to CLDs' C-termini is indispensable for TJ formation (Itoh et al., 1999; Umeda et al., 2006). In addition, we recently demonstrated that phosphatidylinositol phosphates (PIPs) can act as the endogenous competitor of ZO-1(PDZ1)-CLDs interaction, thereby reducing TJ-integrity (Hiroaki et al., 2018). It should be noted that the intracellular concentration of PIPs negatively correlated to TJ-integrity in variety of the cells. For example, increased PIPs concentration induced by inhibition of either PLCγ (Balda et al., 1991) or PLCβ (Balda et

al., 1993) might promoted to decrease TJ integrity. Accordingly, increase of internal PIPs concentration induced by activation of PI3K by perfluorooctane sulfonate increased the permeability of the blood–brain barrier (BBB) (Wang et al., 2011), whereas in, the BBB permeability was reduced significantly by knockout of PI3Kγ (Jin et al., 2011). There is another example, disruption of TJ-integrity at NSAIDs-induced colitis cases (Takeuchi and Satoh, 2015). We also found that one of NSAIDs, such as diclofenac, accidentally bind to ZO-1(PDZ1) (Tenno et al., 2013). This direct interaction is partly consistent as a potential molecular mechanism of diclofenac-induced intestinal permeability change (Yamashita et al., 1985), although NSAID-induced intestinal damage was linked to inhibition of cyclooxygenase 1 and 2 by the drug. Nevertheless, the affinities between these flavonoids and PDZ domain are not strong enough to explain the pharmacological activity; thus, we considered that other signaling pathways must exist. We focused on two related signaling pathways, namely, the TGF-β/ALK-5/Smad pathway and MEK/ERK pathway. These two pathways were shown to be involved in either CLD-2 downregulation or fibroblast-like change of cell morphology. A possible molecular mechanism by baicalin and baicalein in TJ mitigation and morphological change in MDCK cells is summarized in Fig. 10.

Pharmacological actions of many naturally occurring flavonoids against TJs have been extensively studied. However, most of these studies were performed in the context of preservation of intestinal barrier function rather than applications of drug absorption enhancer with TJ-mitigating activity. To date, many flavonoids have been reported to tighten TJs and strengthen the intestinal barrier function or protect/preserve TJs' integrity and barrier function against various types of pathological stimulation. The examples of TJ-tightening flavonoids include quercetin (Amasheh et al., 2008; Suzuki and Hara, 2011, 2009); myricetin (Suzuki and Hara, 2009); kaempferol (Suzuki et al., 2011); soy isoflavones, especially genistein (Suzuki and Hara, 2011); and astilbin (Nakahara et al., 2017). In addition, enhancement of intestinal barrier function was also reported for some flavonoids, namely, naringenin (Noda et al., 2013) and biochanin A (Piegholdt et al., 2014). Some flavonoids are also known to exhibit protective or preserving activity of the epithelial barrier function in the context of several pathologic stimulations, such as quercetin (against H_2O_2 treatment; Chuenkitiyanon et al. 2010); pinocembrin (against dextran-sulfate

sodium treatment; Hu et al. 2019); and orange peel flavonoids, including naringenin (against alcohol stress; Chen and Kitts 2017). In contrast, any flavonoids with TJ-mitigation activity on MDCK II cells, such as baicalin and baicalein, have not been reported to date. Thus, our findings may bring a novel insight into either basic pharmacology or application of the Chinese skullcap-derived flavonoids.

Finally, we demonstrated the potential of baicalin and baicalein as drug absorption enhancers via the paracellular pathway by mildly opening the TJs. Although baicalin and baicalein could partly activated TGF-β signaling pathway, they did not complete EMT, and ZO-1 and OCLN still remained at TJ area. This suggested that the fundamental architecture of TJ at the cell–cell junction was preserved. Thus, we classified both baicalin and baicalein as TJ mitigators but not TJ-destroying agents. Although our study is limited only to biophysical and in vitro studies, the potential of the clinical use of the flavonoids from Chinese skullcap seems promising. As described above, Chinese skullcap has a long history of medicinal use in China and Japan. Except for hepatotoxicity (Dhanasekaran et al., 2013; Linnebur et al., 2010), there are no severe health claims related to the administration of Chinese skullcap extract (Makino et al., 2008). In this study, we also demonstrated that the extracts mainly contained both baicalin and baicalein in a varied content that depended on the difference of extraction methods. Accordingly, we recommend using baicalin and baicalin-rich extract rather than baicalein, because baicalein exhibited an unexpected morphological transition into the slender fibroblast-like shape. The molecular mechanism of this morphological change remains unclear, although we partly demonstrated the involvement of ALK-5. Additional toxicological study of baicalein to epithelial cells should be conducted.

5. Conclusion

In this study, we demonstrated that baicalin, baicalein and the polyphenolic extracts from *Radix scutellariae* can mitigate the tight junction in MDCK II cells, and furthermore they could loosen epithelial barrier functions in human intestinal CaCo-2 cells. However, both baicalein and baicalein-rich *Radix scutellariae* extract exhibited cell morphology change. We expect that usage of baicalin and baicalin-rich Radix scutellariae extract are useful for drug absorption enhancer via para-cellular pathway.

Acknowledgments: The authors would like to thank Scribendi Editing Services (https://www.scribendi.com/) for the English language review.

Grant Information: This work was supported in part by the Japan Science and Technology Agency (JST), the Target Protein Research Program, Japan Science and Technology Agency, A-step Feasibility Study Program (AS262Z01275Q, AS242Z00566Q), Japan Society for the Promotion of Science KAKENHI (15H04337) and KOSÉ Cosmetology Research Foundation.

Conflicts of Interest: The authors have no conflict of interest, financial or otherwise, in relation to this study

Author Contributions: Conceptualization, H.H., and T.T.; Data Analysis, M. Hisada and T.T.; Investigation, M. Hisada., M.N., M.Hiranuma, N.G., and T.T.; Resources, T.T. and N.G.; Writing-Original Draft Preparation, H.H.; Writing-Review & Editing, H.H.; Visualization, T.T.; Manuscript revision, T.T.; Supervision, H.H.; Project Administration, H.H.; Funding Acquisition, H.H.

References

Adachi, M., Inoko, A., Hata, M., Furuse, K., Umeda, K., Itoh, M., Tsukita, S., 2006. Normal Establishment of Epithelial Tight Junctions in Mice and Cultured Cells Lacking Expression of ZO-3, a Tight-Junction MAGUK Protein. Mol. Cell. Biol. 26, 9003–9015. https://doi.org/10.1128/MCB.01811-05

Aijaz, S., Balda, M.S., Matter, K., 2006. Tight Junctions: Molecular Architecture and Function, in: International Review of Cytology. pp. 261–298. https://doi.org/10.1016/S0074-7696(06)48005-0

Amasheh, M., Schlichter, S., Amasheh, S., Mankertz, J., Zeitz, M., Fromm, M., Schulzke, J.D., 2008. Quercetin enhances epithelial barrier function and increases claudin-4 expression in Caco-2 cells. J. Nutr. 138, 1067–73. https://doi.org/10.1093/jn/138.6.1067

Appleton, B.A., Zhang, Y., Wu, P., Yin, J.P., Hunziker, W., Skelton, N.J., Sidhu, S.S., Wiesmann, C., 2006. Comparative structural analysis of the Erbin PDZ domain and the first PDZ domain of ZO-1. Insights into determinants of PDZ domain specificity. J. Biol. Chem. 281, 22312–22320. https://doi.org/10.1074/jbc.M602901200

Balda, M.S., González-Mariscal, L., Contreras, R.G., Macias-Silva, M., Torres-Marquez, M.E., García-Sáinz, J.A., Cereijido, M., 1991. Assembly and sealing of tight junctions: possible participation of G-proteins, phospholipase C, protein kinase C and calmodulin. J. Membr. Biol. 122, 193–202.

Balda, M.S., Gonzalez-Mariscal, L., Matter, K., Cereijido, M., Anderson, J.M., 1993. Assembly of the tight junction: the role of diacylglycerol. J. Cell Biol. 123, 293–302.

Cai, Y., Ma, W., Xiao, Y., Wu, B., Li, X., Liu, F., Qiu, J., Zhang, G., 2017. High doses of baicalin induces kidney injury and fibrosis through regulating TGF-β/Smad signaling pathway. Toxicol. Appl. Pharmacol. 333, 1–9. https://doi.org/10.1016/j.taap.2017.08.003

Chen, X.M., Kitts, D.D., 2017. Flavonoid composition of orange peel extract ameliorates alcohol-induced tight junction dysfunction in Caco-2 monolayer. Food Chem. Toxicol. 105, 398–406. https://doi.org/10.1016/j.fct.2017.04.009

Chuenkitiyanon, S., Pengsuparp, T., Jianmongkol, S., 2010. Protective effect of quercetin on hydrogen peroxide-induced tight junction disruption. Int. J. Toxicol. 29, 418–24. https://doi.org/10.1177/1091581810366487

Dhanasekaran, R., Owens, V., Sanchez, W., 2013. Chinese skullcap in move free arthritis supplement causes drug induced liver injury and pulmonary infiltrates. Case reports Hepatol. 2013, 965092. https://doi.org/10.1155/2013/965092

Fanning, A.S., Anderson, J.M., 1996. Protein–protein interactions: PDZ domain networks. Curr. Biol. 6, 1385–1388. https://doi.org/10.1016/S0960-9822(96)00737-3

Fanning, A.S., Mitic, L.L., Anderson, J.M., 1999. Transmembrane proteins in the tight junction barrier. J. Am. Soc. Nephrol. 10, 1337–1345.

Förster, C., 2008. Tight junctions and the modulation of barrier function in disease. Histochem. Cell Biol. 130, 55–70. https://doi.org/10.1007/s00418-008-0424-9

Furuse, M., 2009. Knockout animals and natural mutations as experimental and diagnostic tool for studying tight junction functions in vivo. Biochim. Biophys. Acta - Biomembr. 1788, 813–819. https://doi.org/10.1016/j.bbamem.2008.07.017

Furuse, M., Fujita, K., Hiiragi, T., Fujimoto, K., Tsukita, S., 1998. Claudin-1 and -2: novel integral membrane proteins localizing at tight junctions with no sequence similarity to occludin. J. Cell Biol. 141, 1539–50.

Furuse, M., Furuse, K., Sasaki, H., Tsukita, S., 2001. Conversion of zonulae occludentes from tight to leaky strand type by introducing claudin-2 into Madin-Darby canine kidney I cells. J. Cell Biol. 153, 263–72. https://doi.org/10.1083/jcb.153.2.263

Furuse, M., Hata, M., Furuse, K., Yoshida, Y., Haratake, A., Sugitani, Y., Noda, T., Kubo, A., Tsukita, S., 2002. Claudin-based tight junctions are crucial for the mammalian epidermal barrier. J. Cell Biol. 156, 1099–1111. https://doi.org/10.1083/jcb.200110122

González-Mariscal, L., Betanzos, A., Nava, P., Jaramillo, B.E., 2003. Tight junction proteins. Prog. Biophys. Mol. Biol. 81, 1–44.

Harris, B.Z., Lim, W.A., 2001. Mechanism and role of PDZ domains in signaling complex assembly. J. Cell Sci. 114, 3219–3231.

Hiroaki, H., Satomura, K., Goda, N., Nakakura, Y., Hiranuma, M., Tenno, T., Hamada, D., Ikegami, T., 2018. Spatial Overlap of Claudin- and Phosphatidylinositol Phosphate-Binding Sites on the First PDZ Domain of Zonula Occludens 1 Studied by NMR. Molecules 23, 2465. https://doi.org/10.3390/molecules23102465

Hu, L., Wu, C., Zhang, Z., Liu, M., Maruthi Prasad, E., Chen, Y., Wang, K., 2019. Pinocembrin Protects Against Dextran Sulfate Sodium-Induced Rats Colitis by Ameliorating Inflammation, Improving Barrier Function and Modulating Gut Microbiota. Front. Physiol. 10, 908. https://doi.org/10.3389/fphys.2019.00908

Ikenouchi, J., Umeda, K., Tsukita, Sachiko, Furuse, M., Tsukita, Shoichiro, 2007. Requirement of ZO-1 for the formation of belt-like adherens junctions during epithelial cell polarization. J. Cell Biol. 176, 779–86. https://doi.org/10.1083/jcb.200612080

Itoh, M., Furuse, M., Morita, K., Kubota, K., Saitou, M., Tsukita, S., 1999. Direct binding of three tight junction-associated MAGUKs, ZO-1, ZO-2, and ZO-3, with the COOH termini of claudins. J. Cell Biol. 147, 1351–1363.

Jiang, L., Liu, C., Leibly, D., Landau, M., Zhao, M., Hughes, M.P., Eisenberg, D.S., 2013. Structure-based discovery of fiber-binding compounds that reduce the cytotoxicity of amyloid beta. Elife 2, e00857. https://doi.org/10.7554/eLife.00857

Jin, R., Song, Z., Yu, S., Piazza, A., Nanda, A., Penninger, J.M., Granger, D.N., Li, G., 2011. Phosphatidylinositol-3-kinase gamma plays a central role in blood-brain barrier dysfunction in acute experimental stroke. Stroke. 42, 2033–2044. https://doi.org/10.1161/STROKEAHA.110.601369

Li, X., Guo, L., Sun, Y., Zhou, J., Gu, Y., Li, Y., 2010. Baicalein inhibits melanogenesis through activation of the ERK signaling pathway. Int. J. Mol. Med. 25, 923–927. https://doi.org/10.3892/ijmm_00000423

Linnebur, S.A., Rapacchietta, O.C., Vejar, M., 2010. Hepatotoxicity associated with chinese skullcap contained in Move Free Advanced dietary supplement: two case reports and review of the literature. Pharmacotherapy 30, 750–750. https://doi.org/10.1592/phco.30.7.750

Liu, Y., 2010. New insights into epithelial-mesenchymal transition in kidney fibrosis. J. Am. Soc. Nephrol. 21, 212–22. https://doi.org/10.1681/ASN.2008121226

Makino, T., Hishida, A., Goda, Y., Mizukami, H., 2008. Comparison of the major flavonoid content of S. baicalensis, S. lateriflora, and their commercial products. J. Nat. Med. 62, 294–9. https://doi.org/10.1007/s11418-008-0230-7

Nakahara, T., Nishitani, Y., Nishiumi, S., Yoshida, M., Azuma, T., 2017. Astilbin from Engelhardtia chrysolepis enhances intestinal barrier functions in Caco-2 cell monolayers. Eur. J. Pharmacol. 804, 46–51. https://doi.org/10.1016/j.ejphar.2017.03.041

Noda, S., Tanabe, S., Suzuki, T., 2013. Naringenin enhances intestinal barrier function through the expression and cytoskeletal association of tight junction proteins in Caco-2 cells. Mol. Nutr. Food Res. 57, 2019–2028. https://doi.org/10.1002/mnfr.201300045

Nomme, J., Antanasijevic, A., Caffrey, M., Van Itallie, C.M., Anderson, J.M., Fanning, A.S., Lavie, A., 2015. Structural Basis of a Key Factor Regulating the Affinity between the Zonula Occludens First PDZ Domain and Claudins. J. Biol. Chem. 290, 16595–16606. https://doi.org/10.1074/jbc.M115.646695

Paris, L., Tonutti, L., Vannini, C., Bazzoni, G., 2008. Structural organization of the tight junctions. Biochim. Biophys. Acta 1778, 646–59. https://doi.org/10.1016/j.bbamem.2007.08.004

Pei, J., Grishin, N. V., 2014. PROMALS3D: Multiple Protein Sequence Alignment Enhanced with Evolutionary and Three-Dimensional Structural Information, in: Multiple Sequence Alignment Methods. pp. 263–271. https://doi.org/10.1007/978-1-62703-646-7_17

Piegholdt, S., Pallauf, K., Esatbeyoglu, T., Speck, N., Reiss, K., Ruddigkeit, L., Stocker, A., Huebbe, P., Rimbach, G., 2014. Biochanin A and prunetin improve epithelial barrier function in intestinal CaCo-

2 cells via downregulation of ERK, NF-κB, and tyrosine phosphorylation. Free Radic. Biol. Med. 70, 255–264. https://doi.org/10.1016/j.freeradbiomed.2014.02.025

Piotto, M., Saudek, V., Sklenár, V., 1992. Gradient-tailored excitation for single-quantum NMR spectroscopy of aqueous solutions. J. Biomol. NMR 2, 661–665.

Schrödinger, LLC, 2015. The {PyMOL} Molecular Graphics System, Version~1.8.

Schumann, F.H., Riepl, H., Maurer, T., Gronwald, W., Neidig, K.-P., Kalbitzer, H.R., 2007. Combined chemical shift changes and amino acid specific chemical shift mapping of protein-protein interactions. J. Biomol. NMR 39, 275–89. https://doi.org/10.1007/s10858-007-9197-z

Sheng, M., 2001. Molecular organization of the postsynaptic specialization. Proc. Natl. Acad. Sci. U. S. A. 98, 7058–7061. https://doi.org/10.1073/pnas.111146298

Suzuki, T., Hara, H., 2011. Role of flavonoids in intestinal tight junction regulation. J. Nutr. Biochem. 22, 401–408. https://doi.org/10.1016/j.jnutbio.2010.08.001

Suzuki, T., Hara, H., 2009. Quercetin enhances intestinal barrier function through the assembly of zonula occludens-2, occludin, and claudin-1 and the expression of claudin-4 in Caco-2 cells. J. Nutr. 139, 965–74. https://doi.org/10.3945/jn.108.100867

Suzuki, T., Tanabe, S., Hara, H., 2011. Kaempferol enhances intestinal barrier function through the cytoskeletal association and expression of tight junction proteins in Caco-2 cells. J. Nutr. 141, 87–94. https://doi.org/10.3945/jn.110.125633

Takeuchi, K., Satoh, H., 2015. NSAID-induced small intestinal damage - Roles of various pathogenic factors. Digestion. https://doi.org/10.1159/000374106

Tang, W., Sun, X., Fang, J.S., Zhang, M., Sucher, N.J., 2004. Flavonoids from Radix Scutellariae as potential stroke therapeutic agents by targeting the second postsynaptic density 95 (PSD-95)/disc large/zonula occludens-1 (PDZ) domain of PSD-95. Phytomedicine 11, 277–284. https://doi.org/10.1078/0944711041495173

Tenno, T., Goda, N., Umetsu, Y., Ota, M., Kinoshita, K., Hiroaki, H., 2013. Accidental interaction between PDZ domains and diclofenac revealed by NMR-assisted virtual screening. Molecules 18, 9567–81. https://doi.org/10.3390/molecules18089567

Thompson, J.D., Gibson, T.J., Plewniak, F., Jeanmougin, F., Higgins, D.G., 1997. The CLUSTAL_X windows interface: flexible strategies for multiple sequence alignment aided by quality analysis tools. Nucleic Acids Res. 25, 4876–82.

Tsukita, S., Furuse, M., Itoh, M., 2001. Multifunctional strands in tight junctions. Nat. Rev. Mol. Cell Biol. 2, 285–293. https://doi.org/10.1038/35067088

Umeda, K., Ikenouchi, J., Katahira-Tayama, S., Furuse, K., Sasaki, H., Nakayama, M., Matsui, T., Tsukita, Sachiko, Furuse, M., Tsukita, Shoichiro, 2006. ZO-1 and ZO-2 independently determine

where claudins are polymerized in tight-junction strand formation. Cell 126, 741–754. https://doi.org/10.1016/j.cell.2006.06.043

Umetsu, Y., Goda, N., Taniguchi, R., Satomura, K., Ikegami, T., Furuse, M., Hiroaki, H., 2011. 1H, 13C, and 15N resonance assignment of the first PDZ domain of mouse ZO-1. Biomol. NMR Assign. 5, 207–210. https://doi.org/10.1007/s12104-011-9301-x

Wang, X., Li, B., Zhao, W.-D., Liu, Y.-J., Shang, D.-S., Fang, W.-G., Chen, Y.-H., 2011. Perfluorooctane sulfonate triggers tight junction "opening" in brain endothelial cells via phosphatidylinositol 3-kinase. Biochem. Biophys. Res. Commun. 410, 258–263. https://doi.org/10.1016/j.bbrc.2011.05.128

Xie, L., Law, B.K., Chytil, A.M., Brown, K.A., Aakre, M.E., Moses, H.L., 2004. Activation of the Erk Pathway Is Required for TGF-β1-Induced EMT In Vitro. Neoplasia 6, 603–610. https://doi.org/10.1593/neo.04241

Yamashita, S., Saitoh, H., Nakanishi, K., Masada, M., Nadai, T., Kimura, T., 1985. Characterization of enhanced intestinal permeability; electrophysiological study on the effects of diclofenac and ethylenediaminetetraacetic acid. J. Pharm. Pharmacol. 37, 512–3. https://doi.org/10.1111/j.2042-7158.1985.tb03056.x

Zimmermann, P., 2006. The prevalence and significance of PDZ domain-phosphoinositide interactions. Biochim. Biophys. Acta 1761, 947–56. https://doi.org/10.1016/j.bbalip.2006.04.003

Figure Legends

Fig. 1. Multiple sequence alignment and structural comparison of the first PDZ domain of ZO-1 and second PDZ domain of PSD-95. (A) Structure based multiple sequence alignment of selected PDZ domains against crystal structure of mouse ZO-1-PDZ1 (PDB: 4yyx_A). Protein names and accession numbers are as follows: ZO-1 mouse, P39447.2; rat, A0A0G2K2P5; human, Q07157.3; PSD-95 mouse, Q62108.1; rat, P31016.1; and human P78352.3, respectively. The secondary structure of ZO-1(PDZ1) was shown below the sequence. The residues corresponding to the canonical binding pocket were boxed. The sequence alignment was generated by PROMALS3D software (Pei and Grishin, 2014) and colored by ClustalX

(Thompson et al., 1997). Electrostatic surface potential diagrams of (B) ZO-1(PDZ1) and (C) PSD-95(PDZ-2), with positive (blue) and negative (red) electrostatic potentials mapped onto a van der Waals surface diagram of the canonical peptide binding site. Coordinates from PDB codes 4YYX and 3GSL were used, respectively. The color scale ranges between +20 kBT (red) and −20 kBT (blue), where kB is Boltzmann's constant and T is temperature. The canonical binding pockets were hexagonal boxed.

Fig 2. Direct interaction between ZO-1(PDZ1) and the flavonoids from *Radix scutellariae*. Overlaid HSQC spectra of 0.1 mM ZO-1(PDZ1) in the absence (black) and presence of 0.2 mM of baicalin (A) and baicalein (B) (red), respectively. (C) Chemical structure of the selected flavonoids from *Radix scutellariae* used in this study. Normalized chemical shift changes of baicalin (C) and baicalein (D). The changes induced by baicalin and baicalein were mapped to the structure (F, G). Resonances representing residues with larger chemical shift changes than the threshold values are mapped onto the ribbon model of mouse ZO-1(PDZ1) (PDB: 2RRM). The threshold values are indicated by dashed lines in the graphs (D, E). The residues at the interface are displayed in the figure. Normalized chemical shift changes of wogonin (H).

Fig. 3. Effects of baicalin and baicalein on cell shape and tight junction integrity of MDCK II cells. Immunofluorescence staining of CLD-2 (A-E) and bright-field differential interference contrast (DIC) images (F-J) are arrayed. Continuous 96 h exposure by 100 μM baicalin (B, G) and baicalein (D, I) and 48 h exposure by 100 μM baicalin (C, H) and baicalein

(E, J) followed by 48 h incubation in media with DMSO. Scale bar = 20 μm.

Fig. 4. Changes in the amount of protein and mRNA of CLD-2 after 100 μM baicalin or baicalein treatment in MDCK II cells. Western blotting analysis (A, B) and quantitative real-time PCR analysis (C). (A) Reduction of CLD-2 by 48 h treatment with baicalin and baicalein. (B) Restoration of CLD-2 by 48 h incubation without flavonoids after exposure to them. (C) Relative mRNA expression level of CLD-2 after 48 h of baicalin or baicalein treatment.

Fig. 5. DIC and immunofluorescence microscopy of baicalin or baialein-treated MDCK II cells for 48 h. DIC images (A-C), immunofluorescence staining with anti-ZO-1 (D-F) and anti-OCLN (G-I) and rhodamine-phalloidin staining (J-L). Cells were treated with 100 μM baicalin (B, E, H, K) and baicalein (C, F, I, L) for 48 h. Scale bar = 20 μm.

Fig. 6. Effect of ALK-5 inhibitor SB431542 and ERK/MEK inhibitor U0126 against the TJ-mitigating activity of baicalin and baicalein. Immunofluorescence staining with anti-CLD-2 antibody (A) and bright-field DIC images (B) are depicted. Cells were exposed to 100 μM baicalin or 50 μM baicalein for 48 h in the presence or absence of 10 μM SB431542. For U0126, cells were treated flavonoids with above concentration for 45 h and followed by addition of the inhibitor (5 μM) for 3 h. DSO control (a, g) with SB431542 (b) or U0126 (h), baicalin exposure (c, i) with SB431542 (d) or U0126 (j), and baicalein exposure (e, k) with SB431542 (f) or U0126 (l) are arrayed.

Fig. 7. Analysis of cell morphology of living MDCK II cells from DIC images. The treatment for 48 h, continuous 96 h, and 48 h exposure followed by 48 h DMSO wash experiments were analyzed (A, B). The effect of ALK-5 inhibitor SB431542 (10 μM) and ERK/MEK inhibitor U0126 (5 μM) against flavonoids exposure (C, D) were examined. The length of long axis (A, C) and short axis (B, D) are shown.

Fig. 8. Variations of the major flavonoids' content with the different extraction method from the dried chopped *Radix scutellariae* root. Reversed-phase HPLC chart of the simple hot-water extract of *Radix scutellariae* root (A), extraction method A (B) and extraction method B (C) (see text) are shown. Arrows 1–4 indicate baicalin, wogonoside, baicalein, and wogonin. Bright-field DIC images (D-F) and immunofluorescence staining of CLD-2 (G-I) of MDCK II cells are arrayed. Cells were treated with extract A (E, H) and extract B (F, I) for 48 h.

Fig. 9. Paracellular flux of fluorescence-labeled insulin of Caco-2 monolayer cells treated with 300 μM baicalin or baicalein for 24 h.

Fig. 10. Potential molecular mechanisms of baicalin and baicalein with the downregulation of the integrity of tight junctions. (A) Our primary working hypothesis based on the PDZ-domain-derived competitive interaction between CLD-2 and ZO-1 or LNX1. When *Radix scutellariae* flavonoids interfere with the contact of ZO-1 to CLD-2, LNX1 excessively promotes ubiquitination and endocytosis of CLD-2 from the membrane; thus, tight junctions are downregulated. (B) Potential contribution of the other known and unknown signaling pathways that caused tight junction downregulation and partly irreversible cell-shape changes.

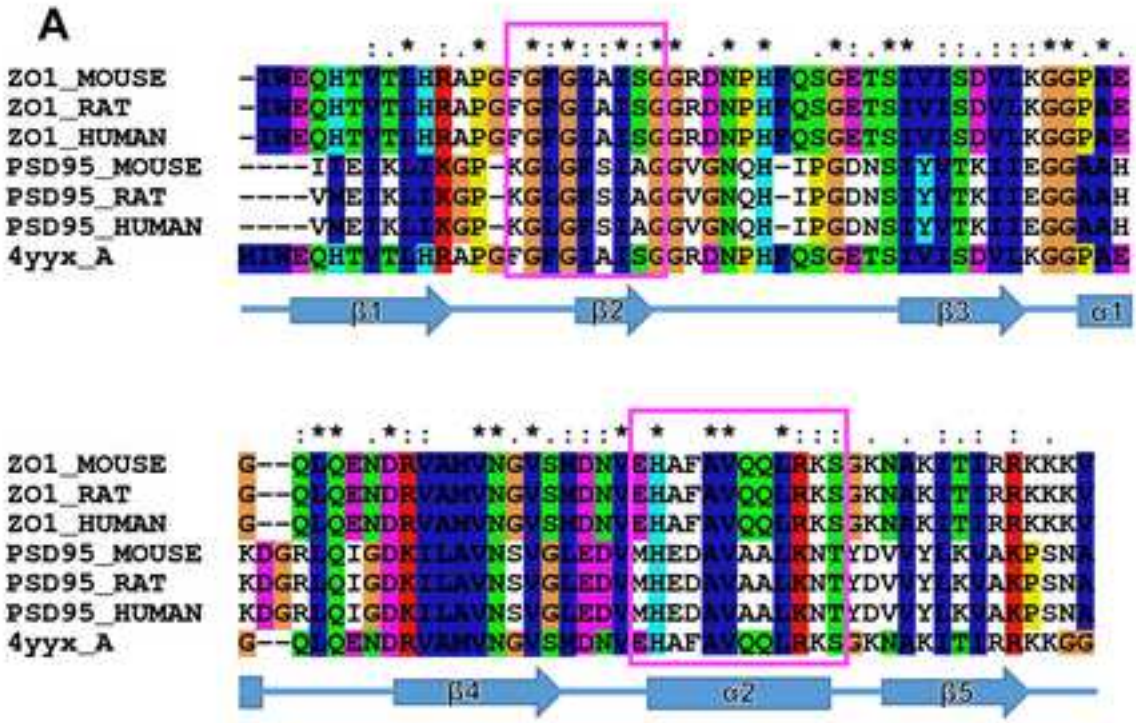
A
ZO1_MOUSE
ZO1_RAT
ZO1_HUMAN
PSD95_MOUSE
PSD95_RAT
PSD95_HUMAN
4yyx_A
β1
β2
β3
α1
β4
α2
β5

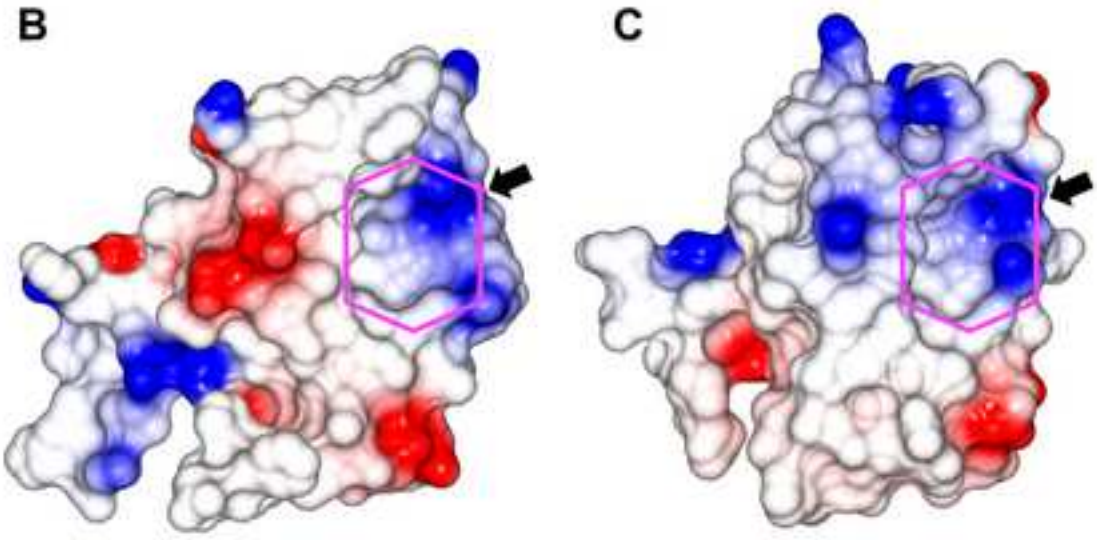
B
C

Fig. 1.

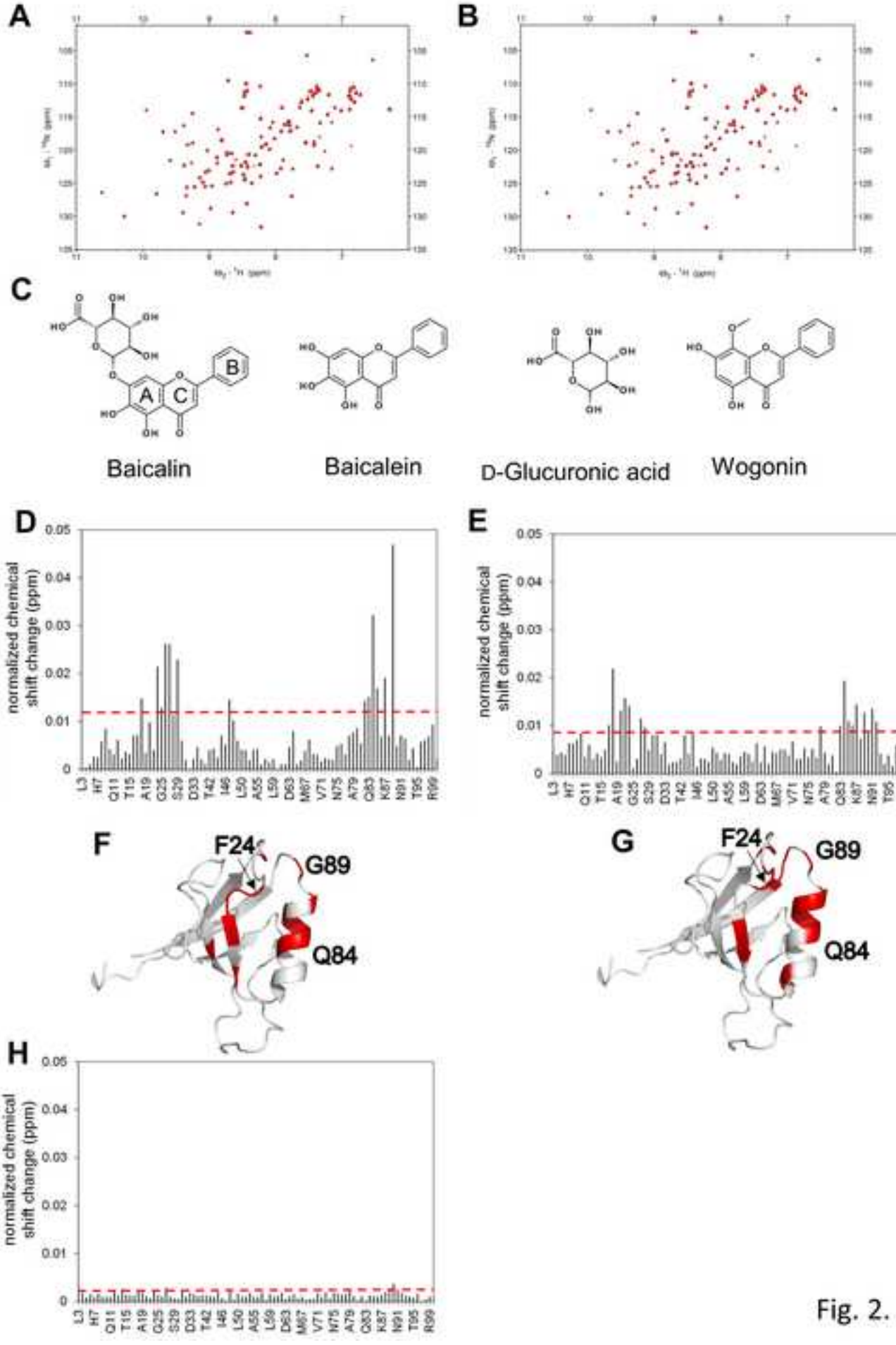
A
B
C
Baicalin
Baicalein
D-Glucuronic acid
Wogonin
D
E
normalized chemical shift change (ppm)
0.05
0.04
0.03
0.02
0.01
0
L3 H7 Q11 T15 A19 G25 S29 D33 T42 I46 L50 A55 L59 D63 M67 V71 N75 A79 Q83 K87 N91 T95 R99
F
G
F24
G89
Q84
H

Fig. 2.

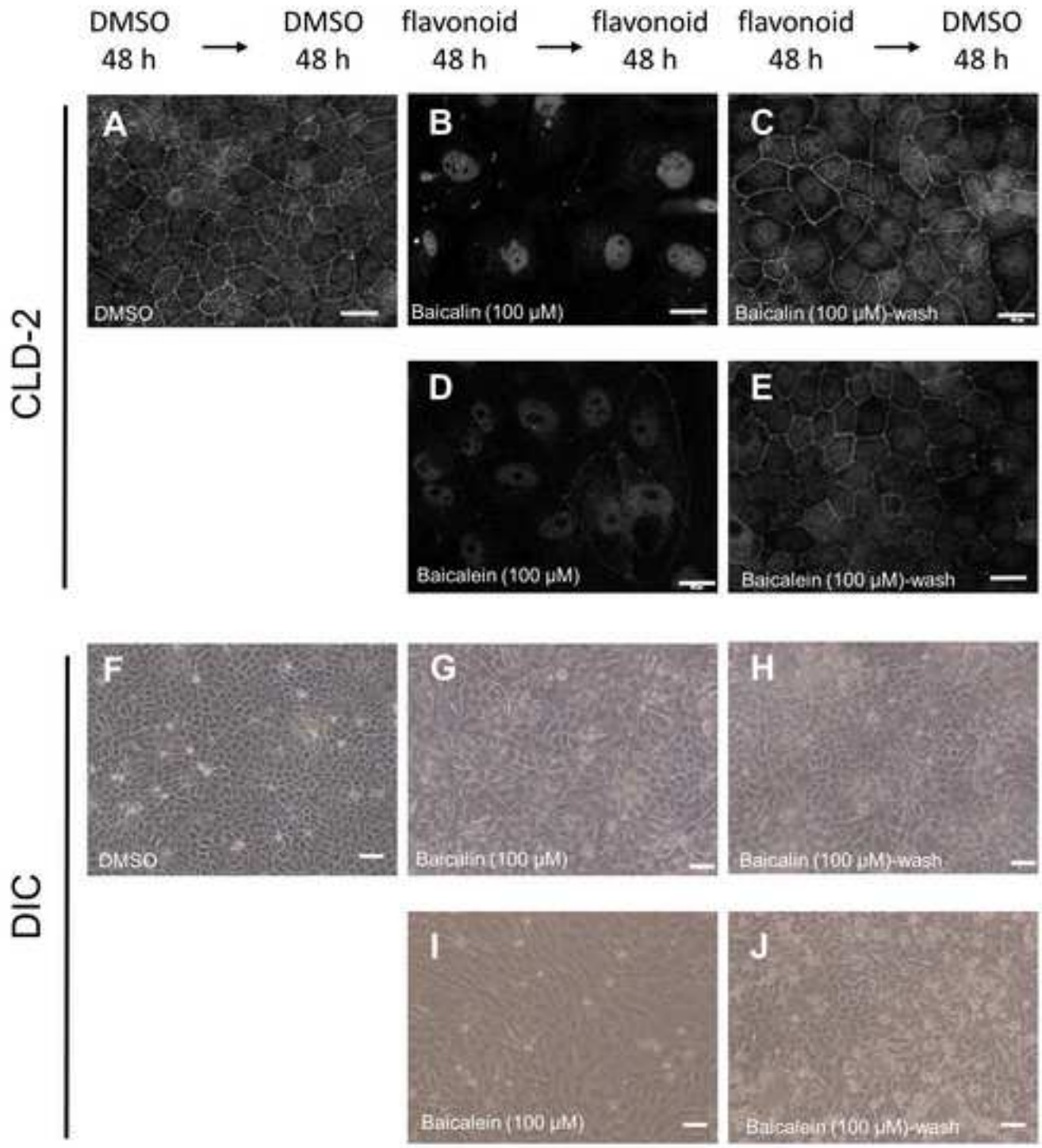
DMSO
48 h
DMSO
48 h
flavonoid
48 h
flavonoid
48 h
flavonoid
48 h
DMSO
48 h
CLD-2
DIC
A
DMSO
B
Baicalin (100 μM)
C
Baicalin (100 μM)-wash
D
Baicalein (100 μM)
E
Baicalein (100 μM)-wash
F
DMSO
G
Baicalin (100 μM)
H
Baicalin (100 μM)-wash
I
Baicalein (100 μM)
J
Baicalein (100 μM)-wash

Fig. 3.

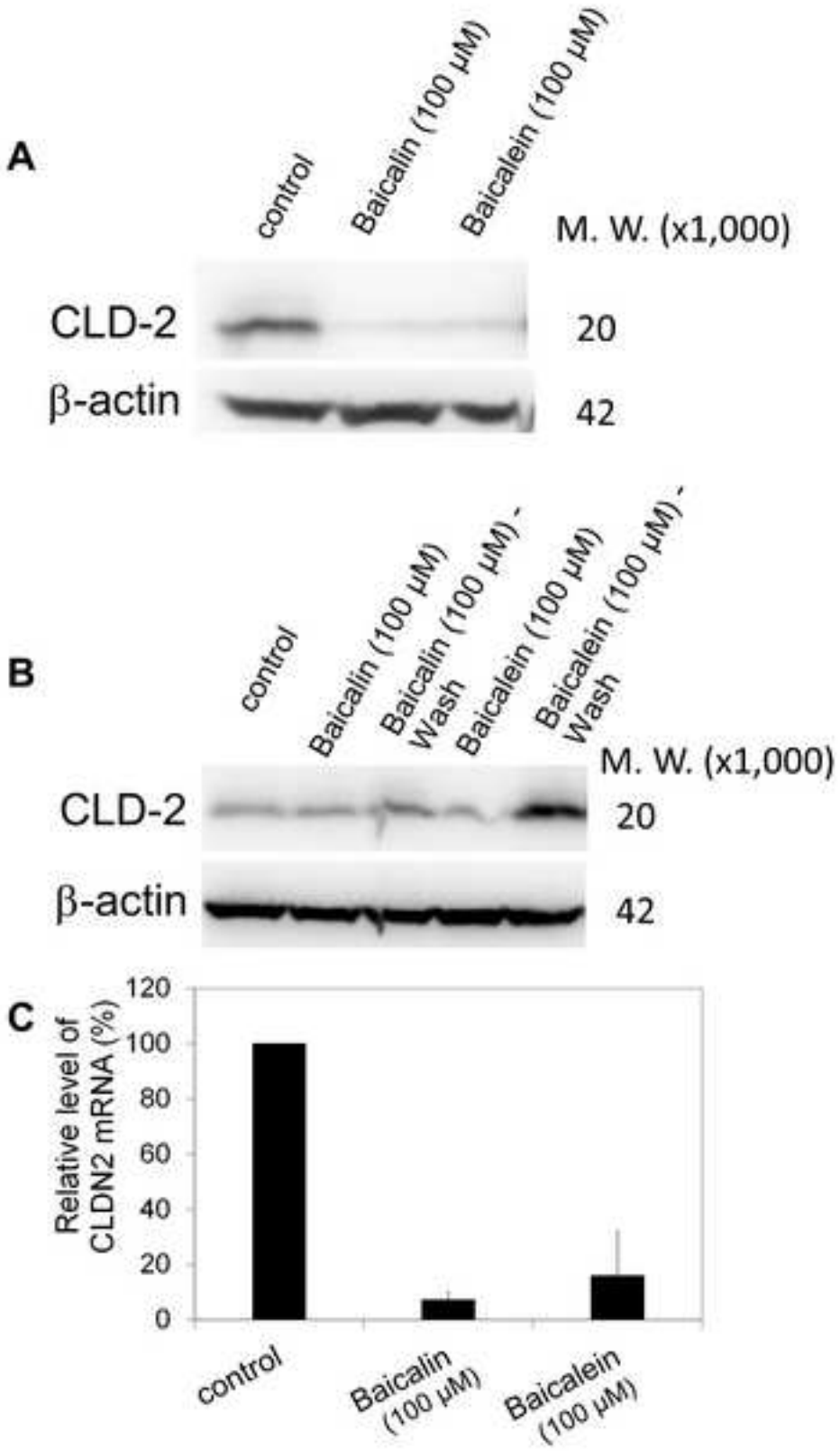
A
control
Baicalin (100 μM)
Baicalein (100 μM)
M. W. (x1,000)
CLD-2
20
β-actin
42
B
control
Baicalin (100 μM)
Baicalin (100 μM) - Wash
Baicalein (100 μM)
Baicalein (100 μM) - Wash
M. W. (x1,000)
CLD-2
20
β-actin
42
C
Relative level of CLDN2 mRNA (%)
120
100
80
60
40
20
0
control
Baicalin (100 μM)
Baicalein (100 μM)

Fig. 4.

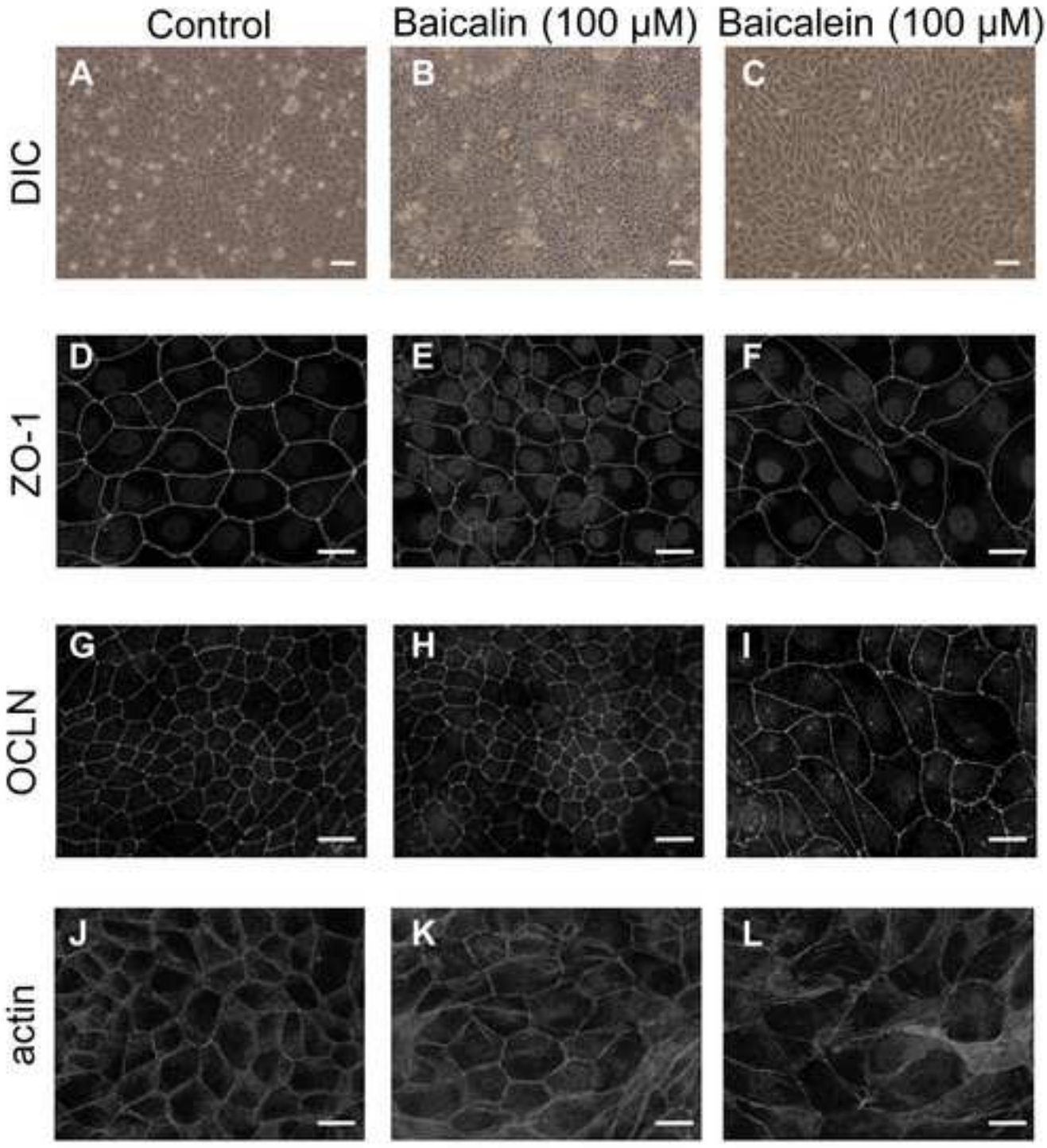
Control
Baicalin (100 μM)
Baicalein (100 μM)
DIC
ZO-1
OCLN
actin
A
B
C
D
E
F
G
H
I
J
K
L

Fig. 5.

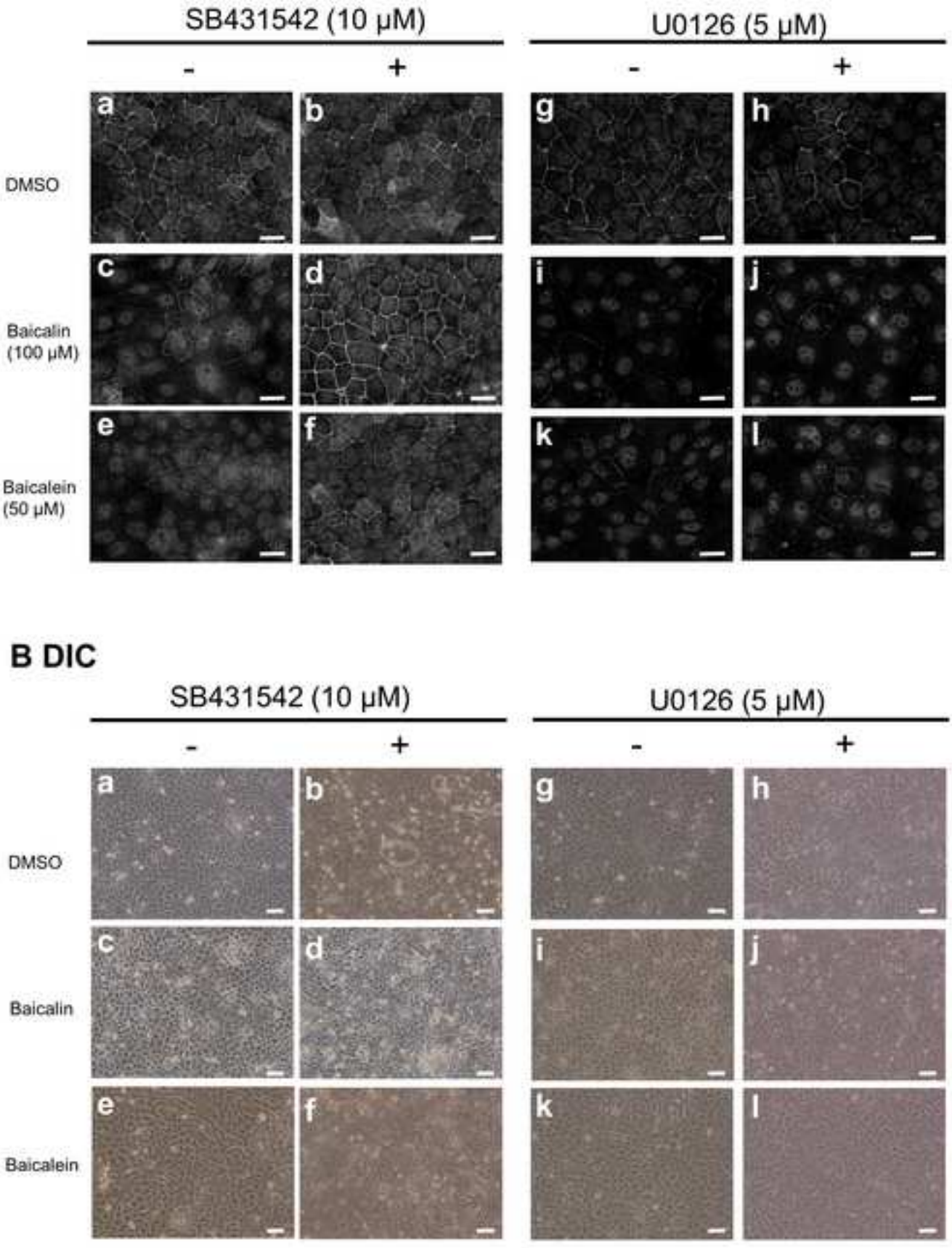
A CLD2
SB431542 (10 μM)
U0126 (5 μM)
-
+
-
+
DMSO
Baicalin (100 μM)
Baicalein (50 μM)
a
b
g
h
c
d
i
j
e
f
k
l
B DIC
SB431542 (10 μM)
U0126 (5 μM)
-
+
-
+
DMSO
Baicalin
Baicalein
a
b
g
h
c
d
i
j
e
f
k
l

Fig. 6.

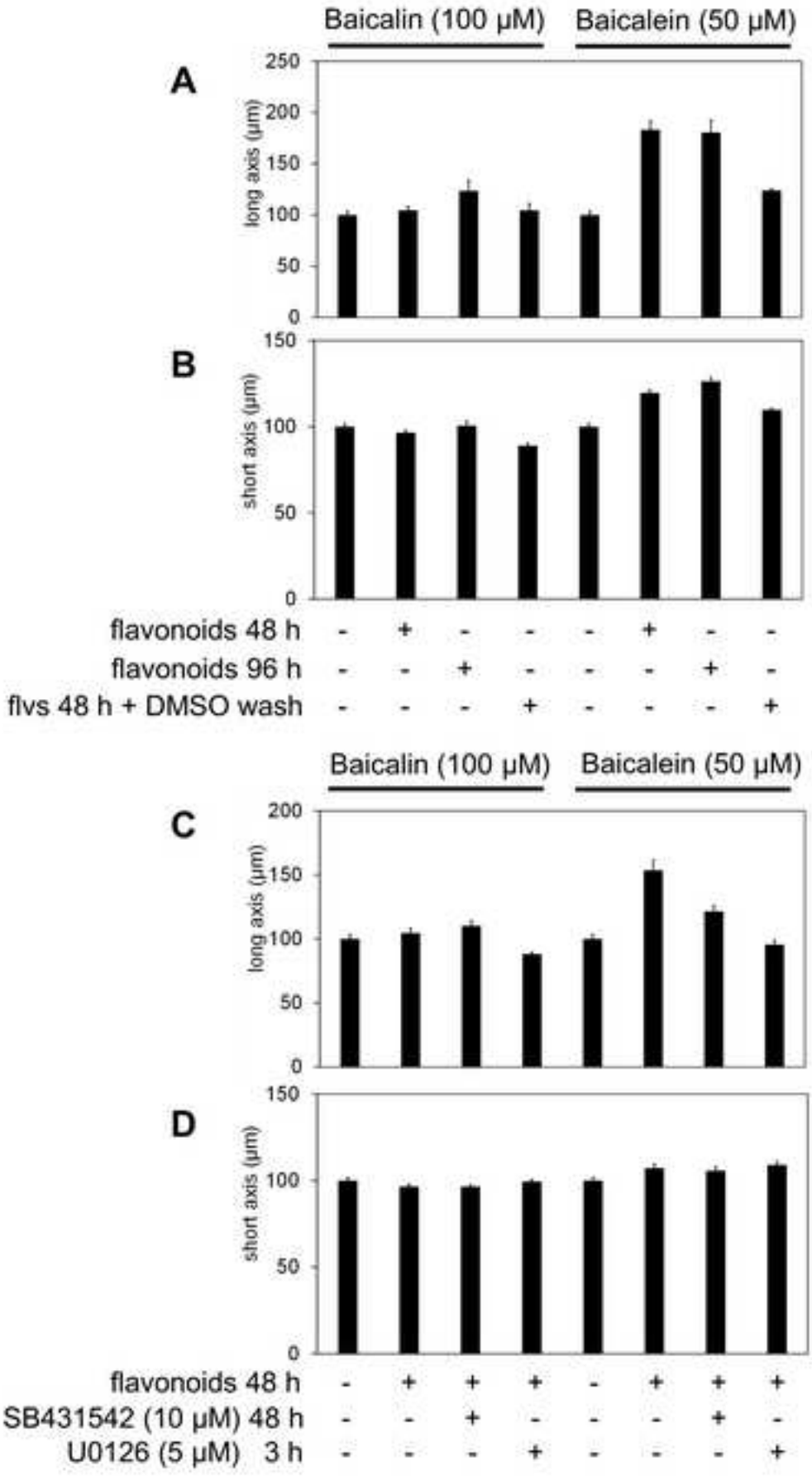
Baicalin (100 μM)
Baicalein (50 μM)
A
long axis (μm)
250
200
150
100
50
0
B
short axis (μm)
150
100
50
0
flavonoids 48 h - + - - - + - -
flavonoids 96 h - - + - - - + -
flvs 48 h + DMSO wash - - - + - - - +
Baicalin (100 μM)
Baicalein (50 μM)
C
long axis (μm)
200
150
100
50
0
D
short axis (μm)
150
100
50
0
flavonoids 48 h - + + + - + + +
SB431542 (10 μM) 48 h - - + - - - + -
U0126 (5 μM) 3 h - - - + - - - +

Fig. 7.

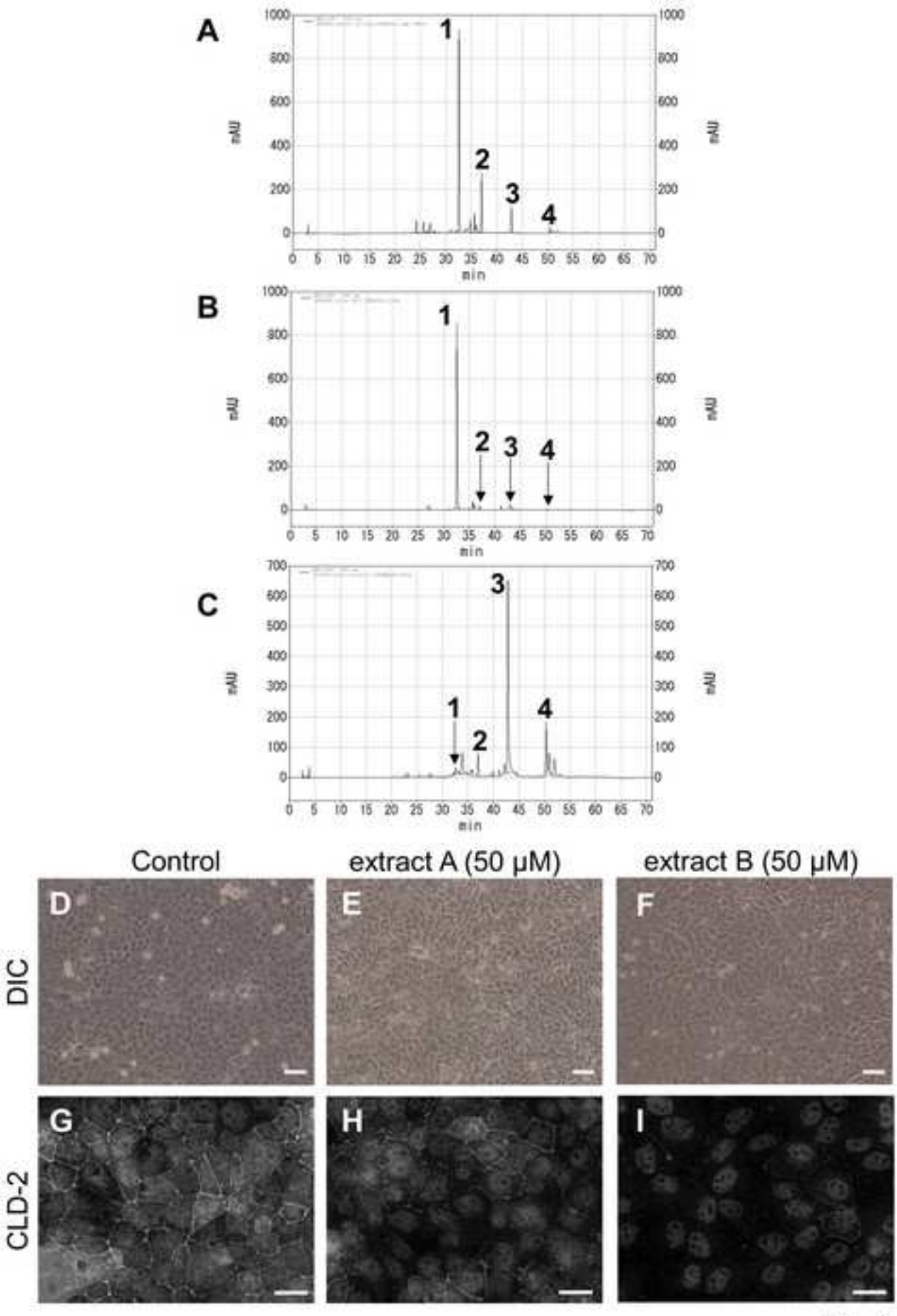
A
B
C
mAU
min
1
2
3
4
Control
extract A (50 μM)
extract B (50 μM)
D
E
F
G
H
I
DIC
CLD-2

Fig. 8.

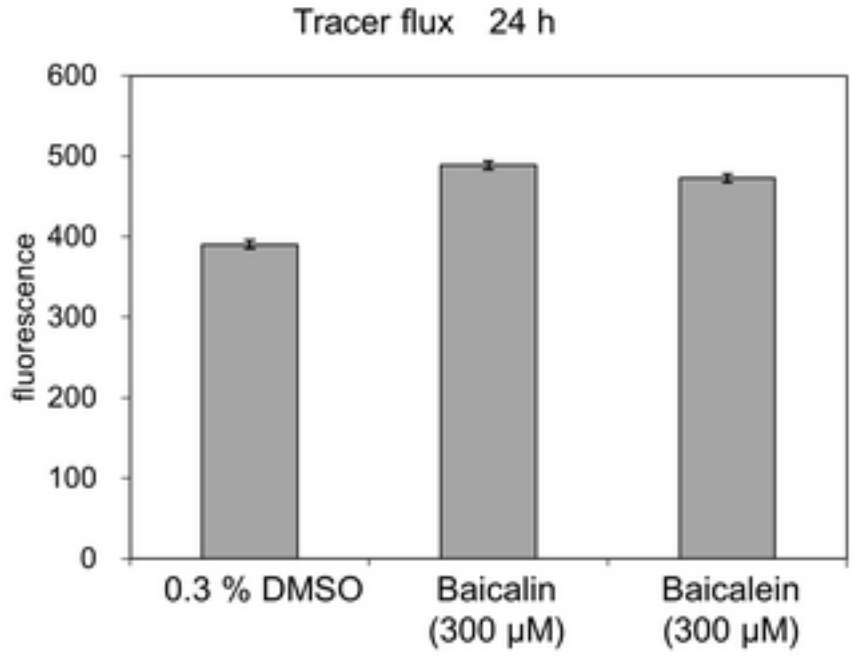
Tracer flux 24 h
600
500
400
300
200
100
0
fluorescence
0.3 % DMSO
Baicalin
(300 µM)
Baicalein
(300 µM)

Fig. 9.

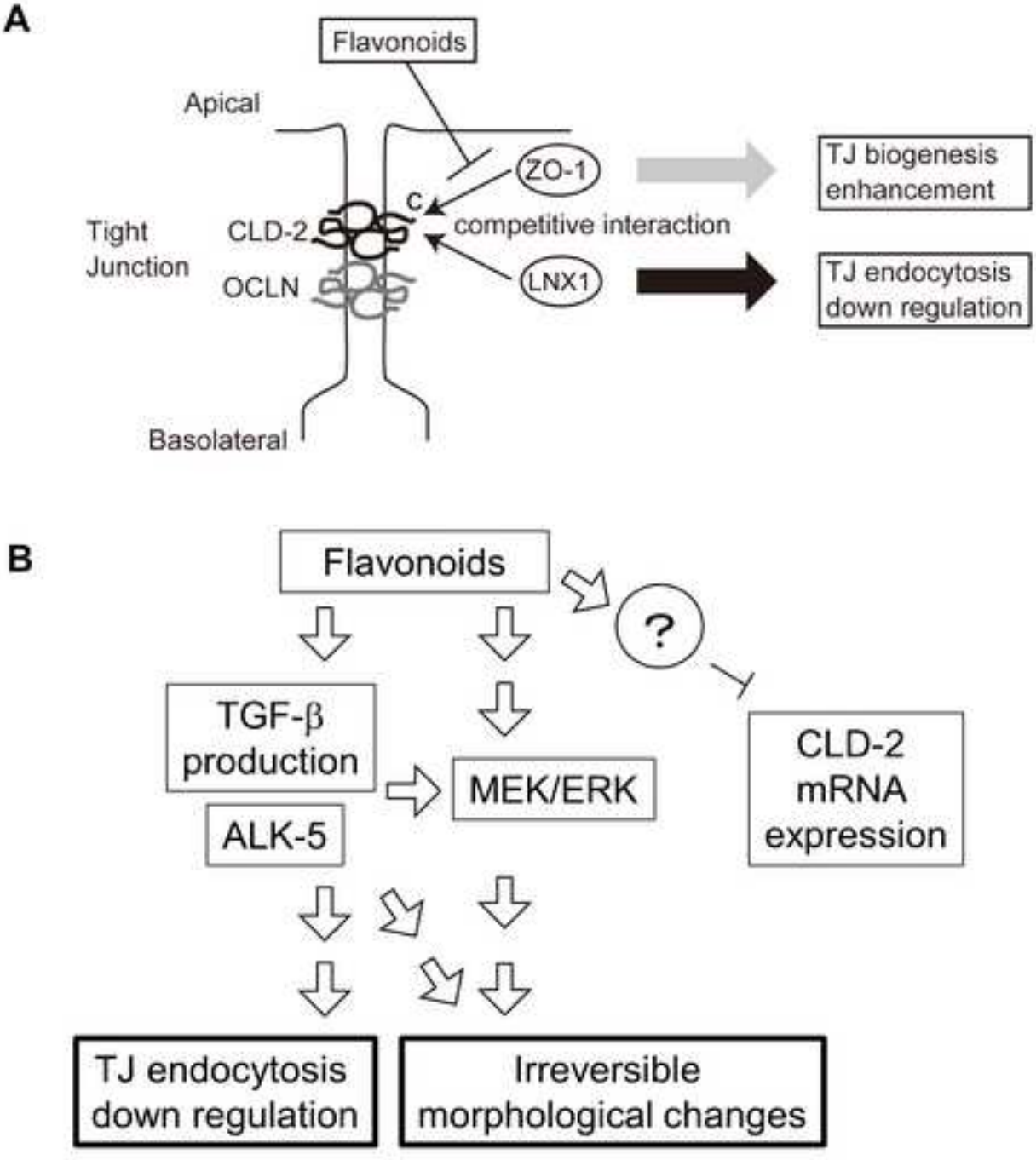
A
Flavonoids
Apical
ZO-1
TJ biogenesis enhancement
C
competitive interaction
Tight Junction
CLD-2
OCLN
LNX1
TJ endocytosis down regulation
Basolateral
B
Flavonoids
?
TGF-β production
MEK/ERK
CLD-2 mRNA expression
ALK-5
TJ endocytosis down regulation
Irreversible morphological changes

Fig. 10.

***Credit Author Statement**

Author Contributions: Conceptualization, H.H., and T.T.; Data Analysis, M. Hisada and T.T.; Investigation, M. Hisada., M.N., M.Hiranuma, N.G., and T.T.; Resources, T.T. and N.G.; Writing-Original Draft Preparation, H.H.; Writing-Review & Editing, H.H.; Visualization, T.T.; Manuscript revision, T.T.; Supervision, H.H.; Project Administration, H.H.; Funding Acquisition, H.H.

SUPPORING INFORMATION

Flavonoids from Chinese skullcap can modulate tight junction integrity by partly targeting the first PDZ domain of zonula occludens-1 (ZO-1)

Misaki Hisada[1], Minami Hiranuma[1], Mio Nakashima[2], Natsuko Goda[1], Takeshi Tenno[1,3], and Hidekazu Hiroaki[1,2,3,*]

1, Graduate School of Pharmaceutical Sciences, Nagoya University, Furocho, Chikusa, Nagoya, Aichi, 464-8601, Japan

2, Department of Biological Sciences, Faculty of Science, Nagoya University

3. BeCerllBar, LLC., Nagoya, Aichi, Japan.

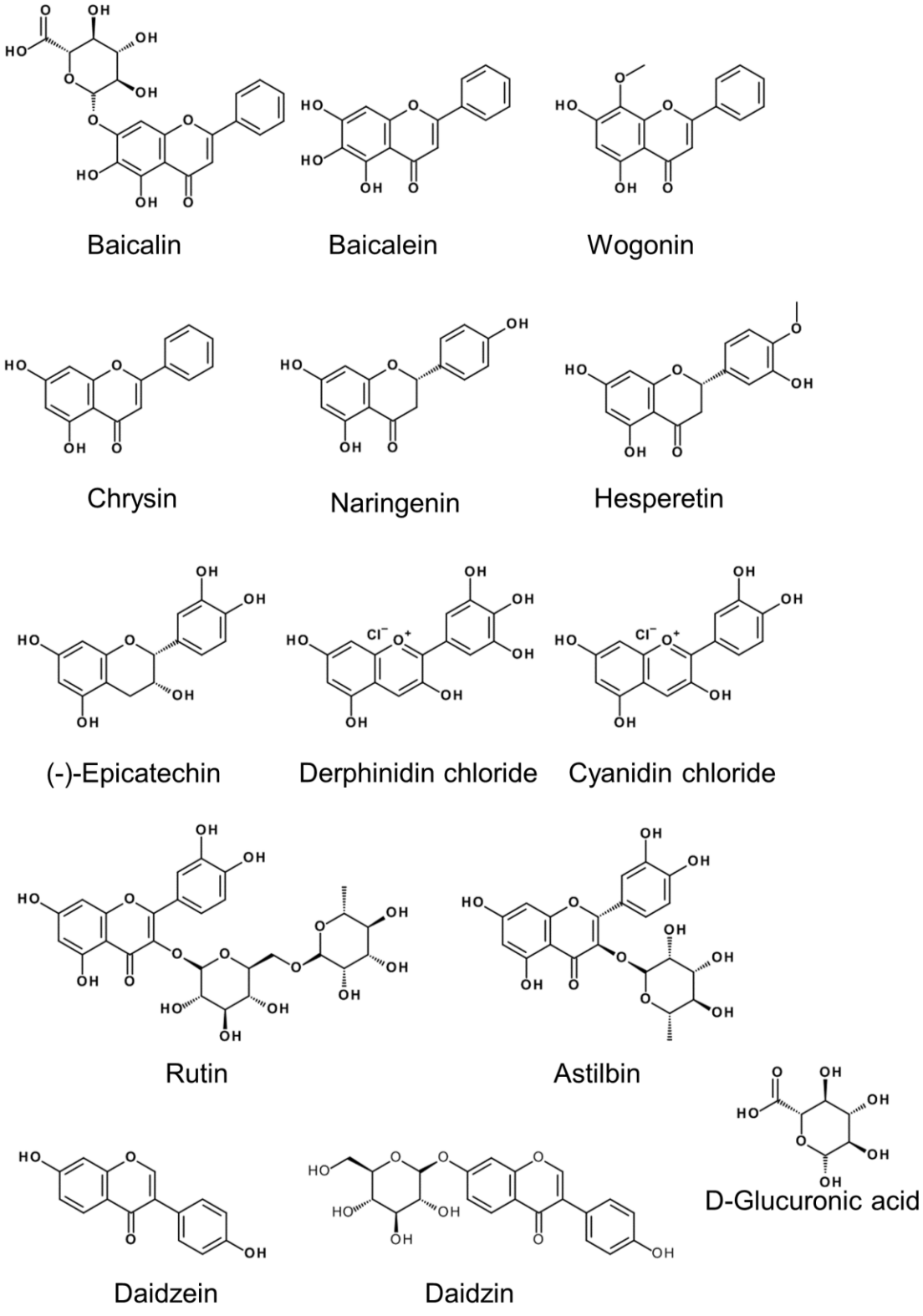

Supplementary Figure 1. Chemical structure of the all selected flavonoids from used in this study.